2021 43rd Annual International Conference of the
IEEE Engineering in Medicine & Biology Society (EMBC)
Oct 31 - Nov 4, 2021. Virtual Conference

Alternating Direction Method of Multipliers Network for Bioluminescence Tomography Reconstruction

Hongbo Guo[1,2], Hengna Zhao[1,2], Xiaolei Song[1,2], Xiaowei He[1,2,*]

Abstract— Bioluminescence tomography (BLT) is an effective noninvasive molecular imaging modality for three dimensional visualization of in vivo tumor research in small animals. The approaches of deep learning have shown great potential in the field of optical molecular imaging in recent years. However, the common problem with these existing end-to-end networks is the black box technology, whose solving process is not theoretically proven. In this work, we proposed a novel Alternating Direction Method of Multipliers Network (ADMM-Net) to solve the poor interpretation problem of internal process. The ADMM-Net combines the framework of deep learning on the basis of traditional ADMM algorithm to dynamically learn various parameters of the algorithm in the form of network. To evaluate the performance of our proposed network, we implemented numerical simulation experiments. The results show that the ADMM-Net can accurately reconstruct the location of the source, and the morphological similarity with the real source is also higher.

I. INTRODUCTION

As a non-contact and non-ionizing imaging modality, bioluminescence imaging (BLI) plays an increasingly significant role in pre-clinical small animal studies [1]. Currently, the applications and value of BLI have been explored in various areas, including exact tumor imaging, monitor tumor growth in vivo and therapy monitoring [2]. Further development of bioluminescence tomography (BLT) has upgraded BLI from planar to three-dimensional (3D) imaging [3]. The 3D bioluminescent sources inside the object body are able to be reconstructed based on the surface optical signals detected by CCD. Mathematically, this inverse process of BLT is inherently ill-posed problem due to more unknowns than number of detectors.

In the past decade, a series of novel strategies have been developed to achieve a more accurate solution. Initially, ℓ_2-norm regularization based reconstruction methods are applied to improve the accuracy of reconstruction [4]. However, the over-smoothness of ℓ_2-norm results reduce high-frequency feature, and lead to blurred or spread targets in the reconstructed images finally. Subsequently, various sparse algorithms have been developed based on the theory of compressed sensing (CS), including adopting a sparse regularization term (e.g. ℓ_0 and ℓ_1), using a greedy strategies [5]–[7]. These algorithms significantly improve the reconstruction accuracy of BLT. Another typical strategy to optimize BLT performance is the combination with prior information. Previous studies have presented that employment of CT anatomical information and divide permissible region could effectively enhance the accuracy and stability of BLT [8]. These promising strategies play crucial roles for BLT development in pre-clinical study.

The recent development of machine learning has shown promising potential in optical molecular imaging. Gao et al. proposed a multilayer perceptron-based inverse problem simulation (IPS) method firstly, which applied in vivo tumor BLT reconstruction to improve the quality [9]. Different from the traditional method, the machine learning method directly models the inverse photon propagation by learning the mapping relation between the surface optical signals and the 3D bioluminescent sources [10]. Since then, other researchers have come up with other deep learning methods in other imaging modality. The two-stage deep learning-based 3D reconstruction algorithm was developed to get less blurry and depth-localized reconstructions by applying a trained 3D convolutional neural network (CNN) in second stage to refine the first stage original fluorescence distribution in fluorescence molecular tomography (FMT) [11]. Besides, Huang et al. presented a novel deep convolutional neural network, gated recurrent unit and multiple layer perception based method (DGMM) for FMT reconstruction with more accurate reconstruction source location [12]. Furthermore, a novel multilayer fully connected neural network (MFCNN) was developed by Zhang et al. to improve the performance of Cerenkov luminescence tomography (CLT) reconstruction with the superiority in terms of accuracy and stability [13]. Guo et al. proposed an end-to-end 3D deep encoder-decoder (3DEnDecoder) network for FMT, and achieved accurate reconstruction results in regular phantom [14]. These thrilling achievements indicate the machine learning has tremendous potential in optical tomography. However, existing based on end-to-end machine learning networks are invisible process with poor interpretability in internal solution. Moreover, the dimension of test data needs to be consistent with the training data, which further limits the development of the networks in practical

*This research is supported by the National Natural Science Foundation of China, Grant/Award Numbers:(61971350, 11871321, 61901374, 61906154, 82071914); Postdoctoral Innovative Talents Support Program, Grant/Award Number: (BX20180254); Project funded by China Post-doctoral Science Foundation, Grant/Award Number: (2018M643719); Science and Technology Plan Program in Xi'an of China, Grant/Award Number: (201805060ZD11CG44);

1 is with the Xi'an Key Laboratory of Radiomics and Intelligent Perception, Xi'an, China.

2 is with the School of Information Sciences and Technology, Northwest University, Xi'an, 710127, China.

∗ is corresponding author (hexw@nwu.edu.cn).

application. Thus, the reconstruction of BLT based on machine learning is still a pressing challenge to be solved.

In this paper, we design the effective deep architectures inspired by Alternating Direction Method of Multipliers (ADMM) algorithm to achieve high-quality BLT reconstruction and overcome poor interpretability problem. This deep architecture, call ADMM-Net, consist of three layers, each of which corresponds to an iteration in ADMM algorithm [15]. Given a surface optical signals data, it flows over the network and outputs a reconstructed data. All the parameters (e.g., penalty parameters, update rates, etc.) in the deep networks can be discriminatively learned from training pairs of surface luminescence data and its true source by L-BFGS optimization and back-propagation over the deep architectures. Simulation experiments demonstrated that the proposed ADMM-Net method achieved accuracy, stability and practicability of BLT reconstruction.

II. Method

A. Photon Propagation Model

The conventional model-based reconstruction depends on the description of photon propagation in biological tissue. Usually, the first-order approximate model of radiative transfer equation (RTE) is utilized to modeling the photon propagation. The diffusion approximation equation can be described as follows:

$$-\nabla \cdot [D(r)\nabla\Phi(r)] + \mu_a(r)\Phi(r) = S(r) \quad r \in \partial\Omega \tag{1}$$

where $D(r)$ is the diffusion coefficient, r is the position vector, $\Phi(r)$ is the photon flux density represents absorption coefficient, $S(r)$ is the source, Ω is the domain under consideration.

In order to solve eq.(1), based on the finite element method (FEM), a relationship between the inside bioluminescent source x and the photon flux of luminescence light Φ can be inferred as [16]:

$$Ax{=}\Phi \tag{2}$$

where A is the system matrix of photon propagation.

B. ADMM Algorithm

The above ill-posed problem can also be optimized efficiently by ADMM algorithm. The following solver is general forms of ADMM algorithm:

$$\begin{aligned} &\min_x \left\{ \tfrac{1}{2}\,||Ax-\Phi||_2^2 + \sum_{l=1}^{L} \lambda_l f(z_l) \right\} \\ &s.t. \quad z_l = x, \quad \forall l \in \{1,2,\ldots,L\} \end{aligned} \tag{3}$$

where λ denotes the regularization parameter and f represents regularization terms on x, e.g., l_p-regularizer ($p \in [0,1]$) for a sparse prior.

Its augmented Lagrangian function is:

$$\begin{aligned} &L_\rho(x,z,\alpha) = \tfrac{1}{2}\,||Ax-\Phi||_2^2 + \\ &\sum_{l=1}^{L} \left[\lambda_l z_l + < \alpha_l, x - z_l > + \tfrac{\rho_l}{2}\,||x-z_l||_2^2 \right] \end{aligned} \tag{4}$$

where $\alpha{=}\{\alpha_l\}$ are Lagrangian multipliers representing dual variables and $\rho{=}\{\rho_l\}$ are penalty parameters respectively. For simplicity, we use scaled definition of $\beta_l{=}\left\{\frac{\alpha_l}{\rho_l}\right\}$ ($l \in \{1,2,\ldots,L\}$), in this case, ADMM alternatively optimizes $\{x,z,\beta\}$ by solving the following three subproblems:

$$\begin{cases} \underset{x}{arg\min}\ \tfrac{1}{2}\,||Ax-\Phi||_2^2 + \sum_{l=1}^{L} \tfrac{\rho_l}{2}\,||x+\beta-z_l||_2^2, \\ \underset{z}{arg\min} \sum_{l=1}^{L} \left[\lambda_l g(z_l) + \tfrac{\rho_l}{2}\,||x+\beta-z_l||_2^2 \right], \\ \underset{\beta}{arg\max} \sum_{l=1}^{L} \langle \beta_l, x-z_l \rangle, \end{cases} \tag{5}$$

C. BLT Reconstruction Based on ADMM-Net

In details, our proposed model ADMM-Net consists of three layers: reconstruction layer, nonlinear transformation layer and multiplier update layer, according to three iterations in ADMM algorithm. The network architecture is shown in Fig. 1.

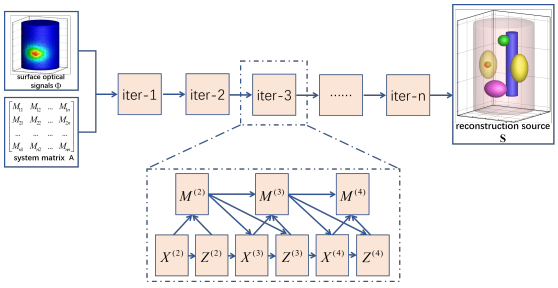

Fig. 1. The network architecture of ADMM-Net.

1) Reconstruction layer $X^{(n)}$: This layer reconstructs a photon intensity after the reconstruction operation. Given the inputs ${z_l}^{(n-1)}$ and ${\beta_l}^{(n-1)}$, the output of this layer is defined as:

$$x^{(n)}{=}[A^{\mathrm{T}}A + \sum_{l=1}^{L} {\rho_l}^{(n)}]^{-1}[A^{\mathrm{T}}\Phi{+}\sum_{l=1}^{L} {\rho_l}^{(n)}({z_l}^{(n-1)}{-}{\beta_l}^{(n-1)})] \tag{6}$$

where $\rho_l^{(n)}$ denotes the l-th penalty parameter, $l{=}1,2,\ldots,L$, and Φ is the photon intensity on the object surface, $z_l^{(0)}$ and $\beta_l^{(0)}$ are initialized to zeros, therefore $x^{(1)} = \left(A^TA + \sum_{l=1}^{L} \rho_l^{(1)}\right)^{-1} \left(A^T\Phi\right)$.

2) Nonlinear transform layer $S^{(n)}$: This layer performs nonlinear transform inspired by the shrinkage function. We aim to learn more general functions using piecewise linear function rather than setting it to be a shrinkage function determined by the regularization term. Given the inputs $\beta_l^{(n-1)}$, the output of this layer is defined as:

$${z_l}^{(n)} = S(x^{(n)} + {\beta_l}^{(n-1)}; \lambda_l/\rho_l) \tag{7}$$

where $S(\cdot)$ is a nonlinear shrinkage function with the parameters λ_l/ρ_l, $\quad l \in \{1,2,\ldots,L\}$.

3) Multiplier update layer $M^{(n)}$: Given inputs $\beta_l^{(n-1)}$, $x_l^{(n)}$ and $z_l^{(n)}$, the output of this layer is defined as:

$$\beta_l^{(n)}=\beta_l^{(n-1)}+\eta_l^{(n)} \times (x_l^{(n)} - z_l^{(n)}) \quad (8)$$

where $\eta_l^{(n)}$ represents an update rate for updating the multiplier.

III. Experiments Setting

A. Simulation Data Set

Different from the end-to-end deep learning network framework, ADMM-Net is a networked algorithm based on formula derivation, with fewer internal parameters and only needs the small sample data set. However, due to the difficulty in obtaining in vivo experimental data, the complexity and time consuming of the experiment, and the difficulty in obtaining the actual distribution of the source in mice. In order to overcome these problems, we utilized the DE method to collect the surface optical signal distribution as training data, and the true source as label. All simulation samples were obtained using a standard cylinder model, which was discretized 1163 nodes and 6237 tetrahedrons, as show in Fig. 2. The organs mainly contain muscle, heart, left lung, right lung, stomach and bone, and the corresponding optical parameters are reference in [16]. Then 100 random points in the right lung region were used as the source to get 100 surface photon intensities as training data set.

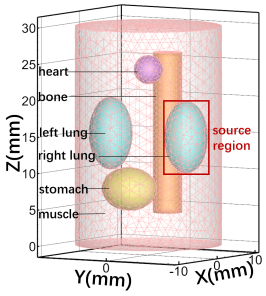

Fig. 2. The model of simulation data set.

B. Numerical Simulation Experiments Setting

In the training data, the light source is a point light source distributed in the right lung region. The single light source experiments were conducted to study the effect of different light source locations on the reconstruction performance of ADMM-Net. The spherical light source with a radius of $1mm$ were implanted in the left lung (0,6,15)mm, stomach (-5, 0, 8)mm and muscle (-5, 0, 20)mm, respectively.

The double sources simulation experiments studied the influence of the distance between the center of the light source on the reconstruction effect. The radius of the two light circles was $1mm$, the distance between the center of the two light sources were $10mm$, $8mm$ and $4mm$, and the distance between the edge and the edge were $8mm$, $6mm$ and $2mm$, respectively. For quantitative assessment, two common indexes were used, including location error (LE) and Dice coefficient [16].

TABLE I
The quantitative results in single source reconstructions.

source location	Recon. location (mm)	LE (mm)	Dice
left lung	(0.05, 6.46, 14.74)	0.53	0.75
stomach	(-5.67, -0.19, 8.11)	0.70	0.70
muscle	(-5.08, 0.16, 19.67)	0.38	0.83

IV. results

1) Single Source: Fig. 3 shows the reconstruction results of the source in different tissues, where (a)-(c) are the 3D reconstruction results of the left lung, stomach and muscle, respectively, and (d)-(f) are the corresponding 2D results display respectively. In 3D, the blue sphere is the real source, and the red area is the reconstructed source. In 2D, the black circle inside is the real source area, while the fluorescent area is the reconstructed source. Tab. I shows the corresponding quantitative analysis indexes. It can see all of three experiments reconstruct the source successfully. When the source is in the left lung, there are large amounts of artifacts and the LE is larger than the other two experiments. And the reconstruction source works best in muscle with LE of $0.38mm$, which is almost identical to the real source with Dice of 0.83.

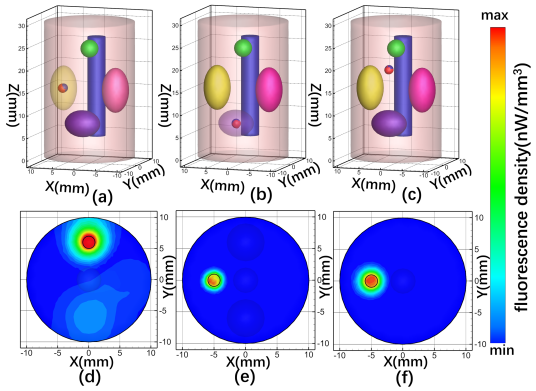

Fig. 3. The reconstruction results of single light source. (a)-(c) are the 3D results of the source in left lung, stomach and muscle, respectively; (d)-(f) are the corresponding 2D cross section.

2) Doubel Sources: Fig. 4 shows the reconstruction results of double sources with different spacing of sources. (a)-(c) are the 3D reconstruction results when the edge-to-edge distance are $8mm$, $6mm$ and $2mm$ respectively. (d)-(f) are the corresponding two-dimensional result display respectively. The blue sphere is the real source, and the yellow area is the reconstructed source. In 2D, the black circle inside is the real source area, while the fluorescent area is the reconstructed source. Tab. II shows the corresponding quantitative analysis indexes. It can

TABLE II

The quantitative results in double sources reconstructions.

distance (mm)	Recon. location (mm)	LE (mm)	Dice
8	(-4.39, 4.68, 15.26)	0.74	0.52
	(-5.85, -5.78, 15.11)	1.16	0.61
6	(-5.06, 4.14, 15.14)	0.20	0.58
	(-5.17, -4.29, 14.64)	0.49	0.79
2	(-5.01, 2.77, 14.97)	0.45	0.52
	(-4.83, -1.93, 15.24)	0.30	0.84

be see that when the distance from edge to edge is the maximum of $8mm$, the reconstruction effect is not as good as that when the distance is $6mm$, which indicates that it is not just the greater the spacing, the better the reconstruction. When the distance from edge to edge is $8mm$, the corresponding LE is the largest, and in the other two cases, the difference between LE and Dice is small with under$0.5mm$. Moreover, when the edge to edge distance is $2mm$, two sources can be reconstructed well, indicating that the spatial resolution of ADMM-Net can reach $2mm$.

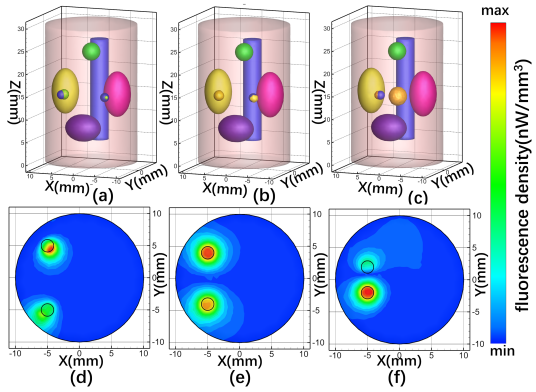

Fig. 4. The reconstruction results of double sources. (a)-(c) are the 3D results with edge-to-edge distances of $8mm$, $6mm$ and $2mm$, respectively; (d)-(f) are the corresponding 2D cross section.

V. CONCLUSIONS

According to iterative solution process of ADMM algorithm, we proposed a novel deep architectures ADMM-Net for BLT in this paper. The ADMM-Net combines the advantages of model-based solution method in integrating knowledge domain with the advantages of deep learning method in effective parameter learning. This novel approach calculates the gradient in reverse process of dynamic learning related parameters, so do not need to set manually. Compared with the model based reconstruction algorithm, the ADMM-Net avoids error caused by improper selection of parameters such as regularization. Compared with the existing machine learning-based methods, the internal solving process is visible, and the algorithm is more interpretable. In addition, there is no restriction on the dimension of training data and test data. It only needs one training to test the data of other different dimensions, which is more applicable.

To verify the performance of ADMM-Net, we design single and double source simulation experiments. The source reconstructed by ADMM-Net has a good effect in terms of morphological similarity, and its Dice value is basically above 0.7, and some groups are even greater than 0.8. Moreover, in the double source experiment, when the distance from edge to edge is $2mm$, the two sources can also be reconstructed well. More simulation experiments based on complex mouse model and in vivo experiments will be conduct to verifiy the performance of ADMM-Net. Beside that, the disadvantage is that the network increases the process of solving the gradient in reverse, which leads to the increase of the complexity of solving and the longer the time needed to consume. Our future work will focus on solving these challenges. We believe that this novel deep architectures of borrowing machine-learning thinking holds great potential of opening a new gate for BLT reconstruction.

References

[1] L. Mezzanotte, M. van't Root, H. Karatas, E. A. Goun, and C. W. Löwik, "In vivo molecular bioluminescence imaging: new tools and applications," Trends in biotechnology, vol. 35, no. 7, pp. 640–652, 2017.

[2] A. C. Obenauf, Y. Zou, A. L. Ji, S. Vanharanta, W. Shu, H. Shi, X. Kong, M. C. Bosenberg, T. Wiesner, N. Rosen et al., "Therapy-induced tumour secretomes promote resistance and tumour progression," Nature, vol. 520, no. 7547, pp. 368–372, 2015.

[3] M. Chehade, A. K. Srivastava, and J. W. Bulte, "Co-registration of bioluminescence tomography, computed tomography, and magnetic resonance imaging for multimodal in vivo stem cell tracking," Tomography, vol. 2, no. 2, p. 158, 2016.

[4] W. Bangerth and A. Joshi, "Adaptive finite element methods for the solution of inverse problems in optical tomography," Inverse Problems, vol. 24, no. 3, p. 034011, 2008.

[5] P. Mohajerani, A. A. Eftekhar, J. Huang, and A. Adibi, "Optimal sparse solution for fluorescent diffuse optical tomography: theory and phantom experimental results," Applied Optics, vol. 46, no. 10, pp. 1679–1685, 2007.

[6] H. Guo, Z. Hu, X. He, X. Zhang, M. Liu, Z. Zhang, X. Shi, S. Zheng, and J. Tian, "Non-convex sparse regularization approach framework for high multiple-source resolution in cerenkov luminescence tomography," Optics Express, vol. 25, no. 23, pp. 28 068–28 085, 2017.

[7] J. Ye, Y. Du, Y. An, C. Chi, and J. Tian, "Reconstruction of fluorescence molecular tomography via a nonmonotone spectral projected gradient pursuit method," Journal of biomedical optics, vol. 19, no. 12, p. 126013, 2014.

[8] Z. Hu, X. Chen, J. Liang, X. Qu, D. Chen, W. Yang, J. Wang, F. Cao, and J. Tian, "Single photon emission computed tomography-guided cerenkov luminescence tomography," Journal of Applied Physics, vol. 112, no. 2, p. 024703, 2012.

[9] Y. Gao, K. Wang, Y. An, S. Jiang, H. Meng, and J. Tian, "Nonmodel-based bioluminescence tomography using a machine-learning reconstruction strategy," Optica, vol. 5, no. 11, pp. 1451–1454, 2018.

[10] H. Meng, Y. Gao, X. Yang, K. Wang, and J. Tian, "K-nearest neighbor based locally connected network for fast morphological reconstruction in fluorescence molecular tomography," IEEE transactions on medical imaging, vol. 39, no. 10, pp. 3019–3028, 2020.

[11] F. Long, "Deep learning-based mesoscopic fluorescence molecular tomography: an in silico study," Journal of Medical Imaging, vol. 5, no. 3, p. 036001, 2018.
[12] C. Huang, H. Meng, Y. Gao, S. Jiang, K. Wang, and J. Tian, "Fast and robust reconstruction method for fluorescence molecular tomography based on deep neural network," in Imaging, Manipulation, and Analysis of Biomolecules, Cells, and Tissues XVII, vol. 10881. International Society for Optics and Photonics, 2019, p. 108811K.
[13] Z. Zhang, M. Cai, Y. Gao, X. Shi, X. Zhang, Z. Hu, and J. Tian, "A novel cerenkov luminescence tomography approach using multilayer fully connected neural network," Physics in Medicine & Biology, vol. 64, no. 24, p. 245010, 2019.
[14] L. Guo, F. Liu, C. Cai, J. Liu, and G. Zhang, "3d deep encoder–decoder network for fluorescence molecular tomography," Optics letters, vol. 44, no. 8, pp. 1892–1895, 2019.
[15] Y. Yang, J. Sun, H. Li, and Z. Xu, "Admm-net: A deep learning approach for compressive sensing mri," arXiv preprint arXiv:1705.06869, 2017.
[16] H. Guo, L. Gao, J. Yu, X. He, H. Wang, J. Zheng, and X. Yang, "Sparse-graph manifold learning method for bioluminescence tomography," Journal of biophotonics, vol. 13, no. 4, p. e201960218, 2020.